

Sign-problem-free Monte Carlo simulation of certain frustrated quantum magnets

Fabien Alet,¹ Kedar Damle,² and Sumiran Pujari³

¹*Laboratoire de Physique Théorique, IRSAMC, Université de Toulouse, CNRS, 31062 Toulouse, France*

²*Department of Theoretical Physics, Tata Institute of Fundamental Research, Mumbai 400 005, India*

³*Department of Physics & Astronomy, University of Kentucky, Lexington, KY-40506-0055*

(Dated: March 6, 2022)

We introduce a Quantum Monte Carlo (QMC) method for efficient sign-problem-free simulations of a broad class of frustrated $S = 1/2$ antiferromagnets using the basis of spin eigenstates of clusters to avoid the severe sign problem faced by other QMC methods. We demonstrate the utility of the method in several cases with competing exchange interactions, and flag important limitations as well as possible extensions of the method.

PACS numbers: 75.10.Jm

Introduction.- Quantum Monte Carlo (QMC) simulations compute equilibrium properties of a many-body system by importance sampling of the canonical partition function $Z = \text{Tr} \exp(-H/T)$, where H is the many-body Hamiltonian, and T is the temperature [1–3]. They have emerged as a major tool for the study of lattice Hamiltonians that either model low- T thermodynamic properties of interesting strongly correlated materials [4, 5], or provide concrete realizations of novel phases in such condensed matter systems [6, 7]. However, models of *geometrically frustrated magnets* [5], in which antiferromagnetic interactions compete with each other due to the geometry of the exchange pathways, have typically remained beyond the reach of QMC methods. This is due to the presence of a *sign problem*, whereby the weights assigned to individual Monte Carlo configurations are no longer strictly positive in the commonly used basis of eigenstates of S_r^z , the z -component of each spin. In such cases, the average sign decreases exponentially with system size and inverse temperature, leading to unmanageably large statistical errors in the estimation of physical quantities. A similar sign-problem crops up in diverse settings ranging from QCD to strongly-correlated metals, and a general solution is considered unlikely [8].

Limited progress has been possible in a few cases, for instance in anisotropic systems in which the frustration only affects S_r^z (thereby allowing sign-free simulation in the z basis [9–17]), or when the sign problem of the full theory can be finessed at low T by working with a low-energy effective Hamiltonian which has no sign problem [18–22]. For some models, sign-free simulations are possible by virtue of specific symmetries of the Hamiltonian [23–29]. In other strongly correlated systems with a full-fledged sign problem, progress has been made in some cases by developing *improved estimators* for computing physical observables [30–33]. In principle, one could also try to find an alternate basis in which all configurations have positive weights. However, this has been possible only in a few interesting cases [34, 35], including some models of topologically ordered states of matter [36–38].

Synopsis.- In this Letter, we introduce a QMC method

that works in the basis of spin eigenstates of clusters to simulate a large class of frustrated quantum magnets in a provably sign-free manner. We focus our discussion on systems in which the clusters in question are made up of two spin $1/2$ moments (\vec{S}_{Ir} and \vec{S}_{IIr}) located on *layers* I and II at *sites* r of a bipartite Bravais lattice in any spatial dimension (Fig. 1), with Hamiltonian

$$H_{\text{bilayer}} = \sum_{\langle r_a r_b \rangle} (\mathcal{J}_z S_{Ir_a}^z S_{Ir_b}^z + \mathcal{J}_\perp \vec{S}_{Ir_a}^\perp \cdot \vec{S}_{Ir_b}^\perp + \text{I} \leftrightarrow \text{II}) + \sum_{\langle r_a r_b \rangle} (\mathcal{K}_z S_{Ir_a}^z S_{IIr_b}^z + \mathcal{K}_\perp \vec{S}_{Ir_a}^\perp \cdot \vec{S}_{IIr_b}^\perp + \text{I} \leftrightarrow \text{II}) + \sum_r (\mathcal{D}_z S_{Ir}^z S_{IIr}^z + \mathcal{D}_\perp \vec{S}_{Ir}^\perp \cdot \vec{S}_{IIr}^\perp), \quad (1)$$

where the nearest neighbour links of this Bravais lattice have been denoted by $\langle r_a r_b \rangle$ to emphasize its bipartite nature, and $\vec{S}_{I/IIr}^\perp$ represents the vector formed by the two transverse components (x and y) of these spins. Geometric frustration of the exchange interactions leads to a severe sign problem for other QMC methods whenever $\mathcal{D}_\perp \mathcal{K}_\perp \mathcal{J}_\perp > 0$. Our central result is that such frustration leads to no sign problems in our method whenever the interactions in H_{bilayer} are constrained to satisfy *at least one* of the following three conditions: i) $\mathcal{K}_z = \mathcal{J}_z$, ii) $\mathcal{K}_\perp = \mathcal{J}_\perp$, iii) $\mathcal{K}_\perp = -\mathcal{J}_\perp$. *Fully-frustrated bilayer* systems [39–44], which have infinitely many conserved quantities, represent a special case with i) and ii) both being satisfied. The method also works when the B-sublattice only hosts a single spin $1/2$ moment \vec{S}_{r_b} that couples symmetrically to \vec{S}_{Ir_a} and \vec{S}_{IIr_a} on neighbouring A sublattice sites [45–47]:

$$H_{\text{mixed}} = \sum_{\langle r_a r_b \rangle} (\mathcal{J}_z S_{Ir_a}^z S_{r_b}^z + \mathcal{J}_\perp \vec{S}_{Ir_a}^\perp \cdot \vec{S}_{r_b}^\perp + \text{I} \leftrightarrow \text{II}) + \sum_{r_a} (\mathcal{D}_z S_{Ir_a}^z S_{IIr_a}^z + \mathcal{D}_\perp \vec{S}_{Ir_a}^\perp \cdot \vec{S}_{IIr_a}^\perp). \quad (2)$$

For $\mathcal{D}_\perp > 0$, the usual QMC method has a sign problem, which is no longer present in our QMC scheme. Our method is also expected to apply to other such models

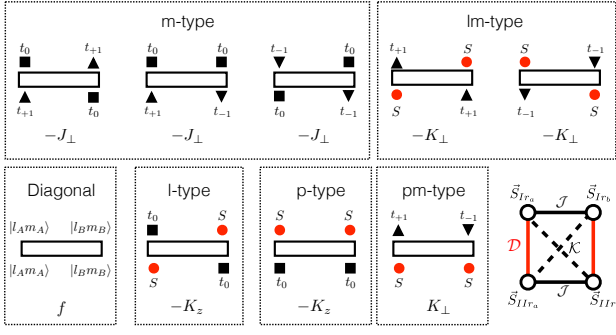


FIG. 1: Vertices that appear in the SSE operator string for H_{bilayer} , with corresponding weights in the canonical cluster basis. All other valid vertices are obtained by symmetry operations that exchange left and right, or upper and lower, legs (keeping the weight fixed). The constant C in the function $f(l_A, l_B, m_A, m_B) = C - J_z m_A m_B - \zeta(\Delta_z - \Delta_\perp)(m_A^2 + m_B^2) - \zeta\Delta_\perp(l_A(l_A + 1) + l_B(l_B + 1))$ is chosen to ensure that $f \geq 0$. Bottom right: Lattice structure and exchange couplings of H_{bilayer} . Vertices and lattice structure for H_{mixed} are detailed in the Supplemental Material.

with infinitely many conserved quantities [48–54]. Additionally, iii) includes interesting examples of frustrated bilayer magnets with full $SU(2)$ symmetry and no extra conservation laws. Some of our results have been obtained independently in recent parallel work [55].

Key idea.— We use the Stochastic Series Expansion (SSE) QMC framework [3] and work at each Bravais lattice site r in the basis $\{|l, m\rangle\}$ of simultaneous eigenstates of the total spin \vec{L}_r^2 and its z component L_r^z , with eigenvalues $l(l+1)$ and m respectively. For H_{bilayer} , we define $\vec{L}_r = \vec{S}_{I_r} + \vec{S}_{II_r}$ on both sublattices. For H_{mixed} , this is modified on the B sublattice by defining $\vec{L}_{r_b} = \vec{S}_{r_b}$. We decompose the Hamiltonian into terms living on bonds $\langle r_a r_b \rangle$ of the bipartite Bravais lattice, with the terms proportional to \mathcal{D}_z and \mathcal{D}_\perp at each site r being shared equally among all bonds emanating from r :

$$\begin{aligned}
 H_{1\langle r_a r_b \rangle} &= J_z L_{r_a}^z L_{r_b}^z + \zeta \Delta_z [(\vec{L}_{r_a}^z)^2 + (\vec{L}_{r_b}^z)^2] \\
 &\quad + \zeta \Delta_\perp [(\vec{L}_{r_a}^\perp)^2 + (\vec{L}_{r_b}^\perp)^2] - C, \\
 H_{2\langle r_a r_b \rangle}^\pm &= \frac{J_\perp}{2} (L_{r_a}^\pm \cdot L_{r_b}^\mp), \\
 H_{3\langle r_a r_b \rangle} &= K_z N_{r_a}^z N_{r_b}^z, \\
 H_{4\langle r_a r_b \rangle}^\pm &= \frac{K_\perp}{2} (N_{r_a}^\pm \cdot N_{r_b}^\mp),
 \end{aligned} \tag{3}$$

with \vec{L}_r^\perp the vector made of transverse (x/y) components of \vec{L}_r , $\vec{N}_r = \vec{S}_{I_r} - \vec{S}_{II_r}$, $L_r^\pm = L_r^x \pm iL_r^y$, $N_r^\pm = N_r^x \pm iN_r^y$, ζ the inverse coordination number of the bipartite lattice, C a constant introduced to ensure negativity of all matrix elements of the *diagonal* operator $H_{1\langle r_a r_b \rangle}$ in our chosen basis, and $\Delta_\mu = \mathcal{D}_\mu/2$, $J_\mu = (\mathcal{J}_\mu + \mathcal{K}_\mu)/2$, $K_\mu = (\mathcal{J}_\mu - \mathcal{K}_\mu)/2$ (for $\mu = z, \perp$). Using this decomposition, we have $H_{\text{bilayer}} = \sum_{\langle r_a r_b \rangle} H_{1\langle r_a r_b \rangle} + H_{3\langle r_a r_b \rangle} + H_{2\langle r_a r_b \rangle}^+ +$

$H_{4\langle r_a r_b \rangle}^+ + H_{2\langle r_a r_b \rangle}^- + H_{4\langle r_a r_b \rangle}^- \cdot H_{\text{mixed}}$, when decomposed in the same way, only has analogs of the $H_{1\langle r_a r_b \rangle}$ and $H_{2\langle r_a r_b \rangle}^\pm$ terms (Supplemental Material).

Working within the SSE framework with this decomposition of H_{bilayer} , one writes

$$\begin{aligned}
 Z &= \sum_{n=0}^{\infty} \frac{1}{n! T^n} \sum_{\mathcal{S}_n} \langle \alpha_0 | (-H_n) | \alpha_{n-1} \rangle \langle \alpha_{n-1} | (-H_{n-1}) | \alpha_{n-2} \rangle \dots \\
 &\quad \dots \langle \alpha_1 | (-H_1) | \alpha_0 \rangle,
 \end{aligned} \tag{4}$$

where the sum over *operator-strings* \mathcal{S}_n of length n is implemented by allowing each $|\alpha_j\rangle$ to range over the full basis of states, and each H_j to range over all bond-operators $H_{1\langle r_a r_b \rangle}$, $H_{2\langle r_a r_b \rangle}^\pm$, $H_{3\langle r_a r_b \rangle}$, and $H_{4\langle r_a r_b \rangle}^\pm$. Along with the factor of $1/(n! T^n)$, the product of matrix elements appearing in the summand serves as the Monte Carlo weight of each operator-string, and the QMC simulation proceeds by performing an importance sampling of Z .

Proof of positive-weight property.— Clearly, the weight of an operator string *does not* depend on the choice of arbitrary phase factors attached to individual basis states, since these phase factors cancel in pairs in the product of matrix elements that sets the weight. Fixing these phases, we define the *canonical* cluster basis as follows: $|s\rangle = (|\uparrow_I \downarrow_{II}\rangle - |\downarrow_I \uparrow_{II}\rangle)/\sqrt{2}$, $|t_{+1}\rangle = |\uparrow_I \uparrow_{II}\rangle$, $|t_{-1}\rangle = |\downarrow_I \downarrow_{II}\rangle$, and $|t_0\rangle = (|\uparrow_I \downarrow_{II}\rangle + |\downarrow_I \uparrow_{II}\rangle)/\sqrt{2}$. Next, we classify the off-diagonal matrix elements contributing to the weight of an operator-string into five types (Fig. 1): (i) *m-type processes* that hop one quantum of L^z along link $\langle r_a r_b \rangle$ between two neighbouring triplet clusters, (ii) *l-type processes* that exchange the states $|s\rangle$ and $|t_0\rangle$ of two neighbouring clusters, (iii) *p-type processes* that take neighbouring singlet clusters and promote both to the $|t_0\rangle$ state or vice-versa, (iv) *lm-type processes* that exchange singlet and triplet states of neighbouring clusters and simultaneously hop one quantum of L^z , and (v) *pm-type processes* that take neighbouring singlet clusters to states $|t_{\pm 1}\rangle$ and $|t_{\mp 1}\rangle$ respectively, or vice versa.

All processes of a given type have a fixed sign for the corresponding matrix elements between basis states (Fig. 1). Therefore, a positive weight is guaranteed if \mathcal{N}_t , the number of occurrences (in any string \mathcal{S}_n) of t -type processes, has even parity for each type t . These parities are constrained by the periodicity of the operator-string \mathcal{S}_n , *i.e.* the starting state $|\alpha_0\rangle$ is recovered after the action of n operators. Since pair creation of the l quantum number must be balanced by corresponding pair destruction processes, $\mathcal{N}_p + \mathcal{N}_{pm}$ must be even. Since a bipartite lattice only has loops of even length, the number of occurrences of processes that hop the m quantum number must be even, implying that $\mathcal{N}_m + \mathcal{N}_{pm} + \mathcal{N}_{lm}$ is even. By the same argument applied to the l quantum number, $\mathcal{N}_l + \mathcal{N}_{lm}$ must also be even.

Since $H_{2\langle r_a r_b \rangle}^\pm$ only gives rise to *m*-type processes, while $H_{3\langle r_a r_b \rangle}$ gives rise to *l*-type and *p*-type processes

and $H_{4\langle r_a r_b \rangle}^\pm$ gives rise to lm -type and pm -type processes, $K_\perp = 0$ ($K_z = 0$) implies $N_{lm} = N_{pm} = 0$ ($N_l = N_p = 0$). The periodicity constraints then imply that all nonzero N_t are even in both these cases. As a result, in both these cases, each S_n has positive weight in this QMC scheme *regardless of the sign of all nonzero couplings*. On the other hand, if $J_\perp = 0$, *i.e.* $N_m = 0$, only pm -type processes can create or destroy pairs of $m = \pm 1$ states on neighbouring sites, thus ensuring that N_{pm} is even. Along with the other periodicity constraints, this again implies that all nonzero N_t are even, yielding a sign-problem-free method whenever $J_\perp = 0$, *independent of the sign of other couplings*.

Thus, the Monte Carlo weight is positive for frustrated bilayer magnets with Hamiltonian H_{bilayer} when *at least one* of the following conditions is satisfied: i) $\mathcal{K}_z = \mathcal{J}_z$, ii) $\mathcal{K}_\perp = \mathcal{J}_\perp$, iii) $\mathcal{K}_\perp = -\mathcal{J}_\perp$. When i) and ii) are both satisfied, one obtains fully frustrated bilayer systems [39–44] with infinitely many conservation laws, which can have either SU(2) or U(1) symmetry. Additionally, iii) also contains other examples of SU(2) symmetric frustrated magnets (e.g. for $J_z = J_\perp = 0$, $K_z = K_\perp > 0$ and $\Delta_z = \Delta_\perp < 0$) and no extra conservation laws. A similar argument establishes the absence of a sign problem for H_{mixed} (Supplemental Material).

Alternately, this positive-weight property can be made explicit by switching from the canonical cluster basis to a rotated basis obtained by attaching phase-factors $e^{i\theta_{|lm\rangle} + i\eta_{|lm\rangle}}$ to the states $|l, m\rangle$. Here, the $\theta_{|lm\rangle}$ are r -independent, while the $\eta_{|lm\rangle}$ are 0 on the B sublattice and constant on the A sublattice. These phases are chosen in each of these three generic cases to ensure that every nonzero contribution to the weight in the rotated basis is explicitly positive. For instance, when $K_\perp = 0$, we set $\eta_{|t_\pm\rangle} = \theta_{|l, m\rangle} = 0$ (for all l, m), while independently choosing $\eta_{|s\rangle}$ to be 0 or π and $\eta_{|t_0\rangle}$ to be 0 or π depending on the signs of K_z and J_\perp . The other sign-free cases can be handled with slightly different choices for these phase factors (Supplemental Material). The positive-weight property of H_{mixed} can also be made explicit in the same way (Supplemental Material).

Implementation.— A key advantage of this QMC approach is that the usual SSE framework [3] remains valid with no change in the construction of the diagonal update, and one new feature in the construction of directed loop updates: *Three* different kinds of directed loop updates [56, 57] are now possible, involving changes to the m quantum number, or the l quantum number, or both. Additionally, to improve statistics, one can use parallel tempering [58] as well as an additional local update, which identifies worldlines that are only touched by diagonal vertices, and changes their state using Metropolis-type acceptance probabilities.

Benchmarks.— Our implementation, which incorporates all these updates, has been successfully benchmarked against exact diagonalization in spatial dimen-

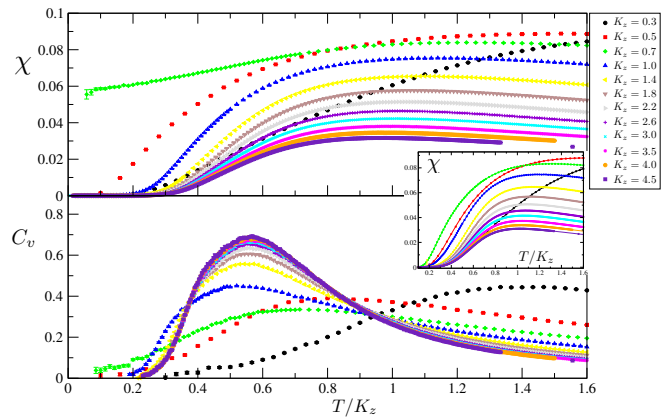


FIG. 2: Temperature (T) dependence of the susceptibility and specific heat of H_{bilayer} with $\mathcal{D}_z = \mathcal{D}_\perp = 1$, $\mathcal{J}_\perp = \mathcal{K}_\perp = 1$, $\mathcal{J}_z = 1 + K_z$, $\mathcal{K}_z = 1 - K_z$. Symbols display data for a sample with $L = 64$ unit cells, plotted for a variety of values of K_z . The inset shows the perfect agreement between QMC data (symbols) and exact diagonalization results (lines) for $L = 6$.

sion $d = 1$ for all the sign-free cases, including the two special cases with infinitely many conserved quantities (Supplemental Material). In Fig. 2 (inset), we illustrate this for a representative example, focusing on the susceptibility $\chi = \beta \langle (S^z)^2 \rangle / N$ and specific heat per spin $C_v = \frac{1}{N} \frac{d\langle H \rangle}{dT}$ for H_{bilayer} in $d = 1$, with $K_\perp = 0$ ($N = 2L$ is the number of spins $1/2$ in a ladder of length L). Data in the main panel illustrate the power of the method, which allows us to access the thermodynamics of this frustrated ladder for fairly large L up to low T , and for a range of values of K_z .

Numerical results in $d=2$.— We now consider H_{bilayer} on a square Bravais lattice in the presence of an additional *magnetic field*, which our method can handle without a sign problem: $H = H_{\text{bilayer}} - h \sum_r (S_{Ir}^z + S_{IIr}^z)$ (the magnetic field only modifies weights of the diagonal vertices). The physics of the fully-frustrated special case ($K_z = K_\perp = 0$) in a certain field range was argued [61] to be dominated at low temperature by sublattice-ordered configurations in which two-spin clusters on one spontaneously chosen sublattice are in the triplet state $|t_{+1}\rangle$, while two-spin clusters on the other sublattice are in a singlet state $|s\rangle$, allowing a low-temperature mapping to the ordered phase of hard squares on the square lattice. This predicts that the system undergoes a temperature-driven phase transition in the 2d Ising universality class to a high-temperature phase in which sublattice symmetry is restored [61, 65].

We have performed a high-precision QMC test of this prediction using a finite-size scaling analysis for samples with up to $N = 2L^2 = 2048$ spins $1/2$, both for the fully-frustrated special case, and in the presence of nonzero K_\perp (previous quantum simulations were limited to $K_\perp = 0$ and $N = 20$). Our determination of the critical value of

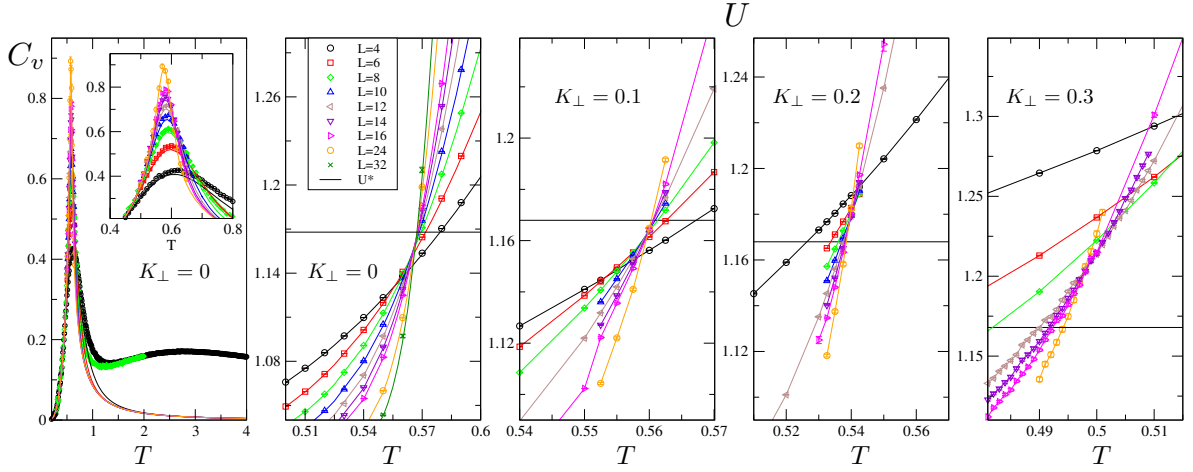


FIG. 3: QMC results (symbols) for H_{bilayer} in a field on the square lattice, with $J_z = K_z = 1$, $\mathcal{D}_z = \mathcal{D}_\perp = 5$, $J_\perp = 1 + K_\perp$, $K_\perp = 1 - K_\perp$, and $h = 7$. Left panel: Specific heat C_v for $K_\perp = 0$ (inset zooms into the critical range). Right panels: Binder cumulant $U = \langle m_s^4 \rangle / \langle m_s^2 \rangle^2$ of the staggered magnetization $m_s = \sum_r (-)^r (S_{I_r}^z + S_{II_r}^z)$. The critical temperature T_c , estimated by the crossing point of U , decreases with K_\perp . U at the estimated T_c tends to the 2d Ising critical value $U^* = 1.16793$ [66] at large L for all K_\perp displayed. The solid lines in the $K_\perp > 0$ panels are guides to the eye. At $K_\perp = 0$, they denote results for the 2d classical Ising model at $T_{\text{ising}} = 4T$.

the Binder cumulant of the staggered magnetization provides clear evidence that this transition indeed belongs to the 2d Ising universality class both for $K_\perp = 0$ and for nonzero K_\perp (albeit with stronger finite-size effects in this case). Indeed, our QMC data for the specific heat and the Binder cumulant close to the phase transition (Fig. 3) are almost identical to those of the classical 2d Ising model when $K_\perp = 0$, but deviate from the classical results outside the critical region, underscoring the nontrivial nature of this correspondence. These deviations become much more significant for nonzero K_\perp . Our method thus enables an investigation of the full parameter regime, including where the hard-square mapping breaks down, both in the fully-frustrated special case and when $K_\perp \neq 0$ (the effect of $K_z \neq 0$ can also be studied).

Discussion.- Clearly, the method presented here can be applied to a large class of frustrated magnets [59–62], and models closely related to specific strongly correlated materials: for instance, a generalized version of H_{mixed} has been argued to be a good model for the mineral azurite $\text{Cu}_3(\text{CO}_3)_2(\text{OH})_2$ [47], and the specific heat of the fully frustrated ladder (Supplemental Material) has similar features with the Shastry-Sutherland compound $\text{SrCu}_2(\text{BO}_3)_2$ [55]. This QMC method also enables the search for finite-T signatures of multi-triplet bond states, as shown in Ref. [55]. Additionally, it offers the possibility of using large-scale unbiased simulations to study interesting quantum phase transitions driven by the competition between different exchange interactions. As we illustrated, a magnetic field (in the z direction) can also be included, thus allowing one to study magnetization processes and plateaux of such frustrated magnets [41, 44, 52, 54]. On the flip-side, we note that this

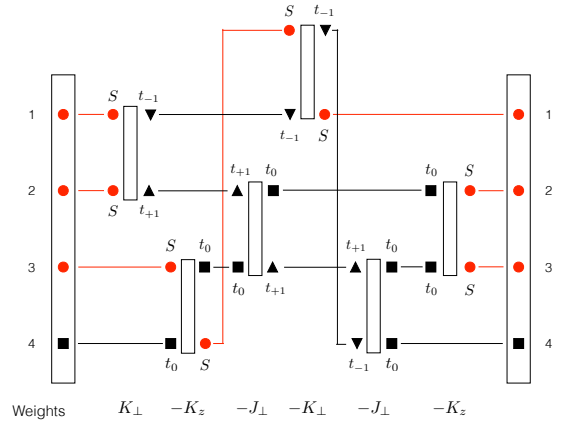


FIG. 4: This operator string for a single plaquette of the Bravais lattice of the bilayer system illustrates the origin of the sign problem faced when simulating the general bilayer Hamiltonian H_{bilayer} : its weight is negative, independent of the signs of the nonzero couplings J_\perp , K_z , and K_\perp .

QMC scheme does *not* remain sign-free when J_\perp , K_\perp and K_z are *all* nonzero in the general bilayer Hamiltonian H_{bilayer} . The simple sequence of processes shown in Fig. 4 for a single plaquette of a square lattice provides an explicit illustration of this limitation. Nevertheless, this construction of negative-weight configurations *relies on the existence of loops* in the underlying bipartite Bravais lattice, and leaves open the possibility that this sign problem could be controlled in 1d systems with open boundaries. To summarize, our work has led to a solution of the sign problem for a large and interesting class of frustrated quantum magnets. Given the ubiquity of the sign problem in computational physics, we hope

that the strategy outlined in this work can be adapted to other systems.

Acknowledgments.— We would like to thank S. Wessel for generously sharing with us some details of the recent parallel work Ref. [55], and for stimulating discussions regarding the sign problem in the general case. We gratefully acknowledge J. Richter for suggesting the study of the finite-temperature Ising transition in the square bilayer system in a field. One of us (KD) would also like to gratefully acknowledge the hospitality of ECT* (Trento), ICTP (Trieste), and ICTS-TIFR (Bengaluru) during the writing of this manuscript. This work was supported by the Indo-French Centre for the Promotion of Advanced Research (IFCPAR/CEFIPRA Project 4504-1), and performed using numerical resources from GENCI (grants 2014-x2014050225 and 2015-x2015050225) and CALMIP. Our QMC code is based on the SSE code of the ALPS libraries [67, 68].

-
- [1] “Strongly Correlated Systems Numerical Methods”, A. Avella and F. Mancini (eds.), Springer Series in Solid State Sciences Vol. 176, Springer Berlin Heidelberg (2013).
 - [2] “Algorithms and Computations”, W. Krauth, Oxford Master Series in Statistical Computational and Theoretical Physics, Oxford University Press (Oxford, 2006).
 - [3] “Computational Studies of Quantum Spin Systems”, A.W. Sandvik, AIP Conf. Proc. **1297**, 135 (2010).
 - [4] “Thermodynamics of Spin $S = 1/2$ Antiferromagnetic Uniform and Alternating-Exchange Heisenberg Chains”, D.C. Johnston, R.K. Kremer, M. Troyer, X. Wang, A. Klümper, S.L. Bud’ko, A.F. Panchula, and P.C. Canfield, Phys. Rev. B **61**, 9558 (2000).
 - [5] “Introduction to Frustrated Magnetism Materials, Experiments, Theory”, C. Lacroix, P. Mendels and F. Mila (eds.), Springer Series in Solid State Sciences Vol. 176, Springer Berlin Heidelberg (2011).
 - [6] “Monte Carlo Simulations of Quantum Spin Models”, S. Wessel in Lecture Notes of the Autumn School Correlated Electrons 2013, “Emergent Phenomena in Correlated Matter”, E. Pavarini, E. Koch, and U. Schollwöck (eds.), Forschungszentrum Jülich (2013).
 - [7] “Bridging lattice-scale physics and continuum field theory with quantum Monte Carlo simulations”, R.K. Kaul, R.G. Melko, and A.W. Sandvik, Annu. Rev. Con. Mat. Phys. **4**, 179 (2013).
 - [8] “Computational complexity and fundamental limitations to fermionic quantum Monte Carlo simulations”, M. Troyer and U.-J. Wiese, Phys.Rev.Lett. **94**, 170201 (2005).
 - [9] “Ising models of quantum frustration”, R. Moessner and S. L. Sondhi, Phys. Rev. B **63**, 224401 (2001).
 - [10] “Interplay of quantum and thermal fluctuations in a frustrated magnet”, S. V. Isakov and R. Moessner, Physical Review B **68**, 104409 (2003).
 - [11] “Supersolid Hard-Core Bosons on the Triangular Lattice”, S. Wessel and M. Troyer, Phys. Rev. Lett. **95**, 127205 (2005).
 - [12] “Persistent Supersolid Phase of Hard-Core Bosons on the Triangular Lattice”, D. Heidarian and K. Damle, Phys. Rev. Lett. **95**, 127206 (2005).
 - [13] “Supersolid Order from Disorder: Hard-Core Bosons on the Triangular Lattice”, R. G. Melko, A. Paramekanti, A. A. Burkov, A. Vishwanath, D. N. Sheng, and L. Balents, Phys. Rev. Lett. **95**, 127207 (2005).
 - [14] “Hard-Core Bosons on the Kagome Lattice: Valence-Bond Solids and Their Quantum Melting”, S. V. Isakov, S. Wessel, R. G. Melko, K. Sengupta, and Y. B. Kim, Phys. Rev. Lett. **97**, 147202 (2006).
 - [15] “Spin-Liquid Phase in a Spin-1/2 Quantum Magnet on the Kagome Lattice”, S. V. Isakov, Yong Baek Kim, and A. Paramekanti, Phys. Rev. Lett. **97**, 207204, (2006).
 - [16] “Unusual Liquid State of Hard-Core Bosons on the Pyrochlore Lattice”, A. Banerjee, S. V. Isakov, K. Damle, and Y. B. Kim, Phys. Rev. Lett. **100**, 047208 (2008).
 - [17] “Superfluid insulator transitions of hard-core bosons on the checkerboard lattice”, A. Sen, K. Damle, and T. Senthil, Phys. Rev. B **76**, 235107 (2007).
 - [18] “Spin Nematics and Magnetization Plateau Transition in Anisotropic Kagome Magnets”, K. Damle and T. Senthil, Phys. Rev. Lett. **97**, 067202 (2006).
 - [19] “Triangular and Kagome Antiferromagnets with a Strong Easy-Axis Anisotropy”, A. Sen, F. Wang, K. Damle, and R. Moessner, Phys. Rev. Lett. **102**, 227001 (2009).
 - [20] “Magnetization Plateaus and Sublattice Ordering in Easy-Axis Kagome Lattice Antiferromagnets”, A. Sen, K. Damle, and A. Vishwanath Phys. Rev. Lett. **100**, 097202 (2008).
 - [21] “Sign-problem-free quantum Monte Carlo of the onset of antiferromagnetism in metals”, E. Berg, M.A. Metlitski, S. Sachdev, Science **338**, 1606 (2012).
 - [22] “Quantum Spin Ices and Topological Phases from Dipolar-Octupolar Doublets on the Pyrochlore Lattice”, Yi-P. Huang, G. Chen, and M. Hermele, Phys. Rev. Lett. **112**, 167203 (2014).
 - [23] “World line and determinantal Quantum Monte Carlo methods for spins, phonons, and electrons”, F. F. Assaad and H. G. Evertz, Heraeus Summer School, Greifswald. Springer Lecture Notes in Physics 739, ed. H. Fehske et al., Springer (2008).
 - [24] “Sufficient condition for absence of the sign problem in the fermionic quantum Monte Carlo algorithm”, C. Wu and S.-C. Zhang, Phys.Rev.B **71**, 155115 (2005).
 - [25] “Entropy dependence of correlations in one-dimensional SU(N) antiferromagnets”, L. Messio and F. Mila, Phys. Rev. Lett. **109**, 205306 (2012).
 - [26] “Solution to sign problems in half-filled spin-polarized electronic systems”, E.F. Huffman and S. Chandrasekharan, Phys. Rev. B **89**, 111101 (2014).
 - [27] “Split orthogonal group: A guiding principle for sign-problem-free fermionic simulations”, L. Wang, Y.-H. Liu, M. Iazzi, M. Troyer and G. Harcos, Phys. Rev. Lett. **115**, 250601 (2015).
 - [28] “Solving the fermion sign problem in quantum Monte Carlo simulations by Majorana representation”, Z.-X. Li, Y.-F. Jiang, and H. Yao, Phys. Rev. B **91**, 241117R (2015).
 - [29] “Majorana positivity and the fermion sign problem of quantum Monte Carlo simulations”, Z. C. Wei, C. Wu, Y. Li, S. Zhang, and T. Xiang, arXiv:1601.01994 (2016).
 - [30] “Sign problem in Monte Carlo simulations of frustrated quantum spin systems” P. Henelius and A. W. Sandvik,

- Phys. Rev. B **62**, 1102 (2000).
- [31] “Meron cluster simulation of the theta vacuum in the 2-d $O(3)$ model”, W. Bietenholz, A. Pochinsky, U.-J. Wiese, Phys. Rev. Lett. **75**, 4524 (1995).
 - [32] “Meron-Cluster Solution of Fermion Sign Problems”, S. Chandrasekharan and U.-J. Wiese, Phys. Rev. Lett. **83**, 3116 (1999).
 - [33] “Nested Cluster Algorithm for Frustrated Quantum Antiferromagnets”, M. Nyfeler, F.-J. Jiang, F. Kämpfer and U.-J. Wiese, Phys. Rev. Lett. **100**, 247206 (2008).
 - [34] “Vanishing of the negative-sign problem of quantum Monte Carlo simulations in one-dimensional frustrated spin systems”, T. Nakamura, Phys. Rev. B **57**, R3197 (1998).
 - [35] “Symmetry-protected topological order and negative-sign problem for $SO(N)$ bilinear-biquadratic chains”, K. Okunishi and K. Harada, Phys. Rev. B **89**, 134422 (2014).
 - [36] “Model of Fractionalization of Faraday Lines in Compact Electrodynamics”, S. D. Geraedts and O. I. Motrunich, Phys. Rev. B **90**, 214505 (2014).
 - [37] “Model Realization and Numerical Studies of a Three-Dimensional Bosonic Topological Insulator and Symmetry-Enriched Topological Phases”, S. D. Geraedts and O. I. Motrunich, Phys. Rev. X **4**, 041049 (2014).
 - [38] “Exact realization of integer and fractional quantum Hall phases in $U(1) \times U(1)$ models in $(2+1)d$ ”, S. D. Geraedts and O. I. Motrunich, Annals of Physics **334**, 288 (2013).
 - [39] “Linked-tetrahedra spin chain: Exact ground state and excitations”, M.P. Gelfand, Phys. Rev. B **43**, 8644 (1991).
 - [40] “Finitely Correlated Generalized Spin Ladders”, A. K. Kolezhuk and H.-J. Mikeska, Int. J. Mod. Phys. B **12**, 2325 (1998).
 - [41] “Magnetization plateaus and jumps in a class of frustrated ladders: A simple route to a complex behaviour”, A. Honecker, F. Mila, and M. Troyer, Eur. Phys. J. B **15**, 227 (2000).
 - [42] “Magnetism of a tetrahedral cluster spin chain”, W. Brenig and K.W. Becker, Phys. Rev. B **64**, 214413 (2001).
 - [43] “Magnetization of coupled spin clusters in ladder geometry”, E. Chattopadhyay and I. Bose, Phys. Rev. B **65**, 134425 (2002).
 - [44] “Low-lying excitations and magnetization process of coupled tetrahedral systems”, K. Totsuka and H.-J. Mikeska, Phys. Rev. B **66**, 054435 (2002).
 - [45] “Ground states with cluster structures in a frustrated Heisenberg chain”, K. Takano, K. Kubo and H. Sakamoto, J. Phys.: Condensed Matter **8**, 6405 (1996).
 - [46] “Mixed Heisenberg chains: I. The ground-state problem”, H. Niggemann, G. Uimin, and J. Zittartz, J. Phys.: Condens. Matter **9**, 9031 (1997).
 - [47] “Dynamic and thermodynamic properties of the generalised diamond chain model for azurite”, A. Honecker, S. Hu, R. Peters and J. Richter, J. Phys.: Condens. Matter **23**, 164211 (2011).
 - [48] “Competition between plaquette and dimer phases in Heisenberg chains”, N.B. Ivanov, J. Richter, Phys. Lett. A **232**, 308 (1997).
 - [49] “The antiferromagnetic spin-1/2 chain with competing dimers and plaquettes: numerical versus exact results”, J. Richter, N.B. Ivanov, J. Schulenburg, J. Phys. Cond. Matter **10**, 3635 (1998).
 - [50] “First-order quantum phase transition in the orthogonal-dimer spin chain”, A. Koga, K. Okunishi, and N. Kawakami, Phys. Rev. B **62**, 5558 (2000).
 - [51] “Test of the frustrated spin-cluster model to describe the low-temperature physics of NaV_2O_5 ”, C. Gros, R. Valentí, J.V. Alvarez, K. Hamacher, and W. Wenzel, Phys. Rev. B **62**, R14617(R) (2000).
 - [52] “Infinite series of magnetization plateaus in the frustrated dimer-plaquette chain”, J. Schulenburg and J. Richter, Phys. Rev. B **65**, 054420 (2002).
 - [53] “Magnetic properties of a spin-1/2 quadrumer chain”, A. Honecker and W. Brenig, Phys. Rev. B **63**, 144416 (2001).
 - [54] “Unconventional magnetization plateaus in a Shastry-Sutherland spin tube”, S.R. Manmana, J.-D. Picon, K.P. Schmidt and F. Mila, EPL **94**, 67004 (2011).
 - [55] “Thermodynamic properties of highly frustrated quantum spin ladders: influence of many-particle bound states”, A. Honecker, S. Wessel, R. Kerkdyk, T. Pruschke, F. Mila, and B. Normand, unpublished.
 - [56] “Quantum Monte Carlo with Directed Loops”, O.F. Syljuåsen, and A.W. Sandvik, Phys. Rev. E **66**, 046701 (2002).
 - [57] “Generalized Directed Loop Method for Quantum Monte Carlo Simulations”, F. Alet, S. Wessel, and M. Troyer, Phys. Rev. E **71**, 036706 (2005).
 - [58] “Exchange Monte Carlo method and application to spin glass simulations”, K. Hukushima, and K. Nemoto, J. Phys. Soc. Jap. **65**, 1604 (1996).
 - [59] “Exact Demonstration of Magnetization Plateaus and First Order Dimer-Néel Phase Transitions in a Modified Shastry-Sutherland Model for $SrCu_2(BO_3)_2$ ”, E. Müller-Hartmann, R.R.P. Singh, C. Knetter, G.S. Uhrig, Phys. Rev. Lett. **84**, 1808 (2000).
 - [60] “Exactly soluble quantum spin models on a double layer: The net spin model”, H. Q. Lin, J. L. Shen, and H. Y. Shik, Phys. Rev. B **66**, 184402 (2002).
 - [61] “Finite-temperature order-disorder phase transition in a frustrated bilayer quantum Heisenberg antiferromagnet in strong magnetic fields”, J. Richter, O. Derzhko, and T. Krokhamalskii, Phys. Rev. B **74**, 144430 (2006).
 - [62] “Analysis of a family of Heisenberg systems with simple eigenfunctions for the ground state and low lying excitations”, J. Rössler and D. Gottlieb, Phys. Rev. B **72**, 024443 (2005).
 - [63] “Residual entropy and spin gap in a one-dimensional frustrated antiferromagnet”, M. Mambrini, J. Trébosch, and F. Mila, Phys. Rev. B **59**, 13806 (1999).
 - [64] “Phase diagram of a coupled tetrahedral Heisenberg model”, O. Rojas and F.C. Alcaraz, Phys. Rev. B **67**, 174401 (2003).
 - [65] “Emergent Ising degrees of freedom in frustrated two-leg ladder and bilayer $s = 1/2$ Heisenberg antiferromagnets”, O. Derzhko, T. Krokhamalskii, and J. Richter, Phys. Rev. B **82**, 214412 (2010).
 - [66] “Universal ratio of magnetization moments in two-dimensional Ising models”, G. Kamieniarz and H.W.J. Blöte, J. Phys. A: Math. Gen. **26**, 201 (1993).
 - [67] “The ALPS project release 1.3: open source software for strongly correlated systems”, A.F. Albuquerque *et al.*, J. Mag. Mag. Mat. **310**, 1187 (2007).
 - [68] “Generalized directed loop method for quantum Monte Carlo simulations”, F. Alet, S. Wessel, and M. Troyer, Phys. Rev. E **71**, 036706 (2005).

Supplemental material for “Sign-problem-free Monte Carlo simulation of certain frustrated quantum magnets”

Decomposition of H_{mixed} and SSE vertices

In order to decompose H_{mixed} into operators that live on links $\langle r_a r_b \rangle$ of the underlying bipartite Bravais lattice, we define

$$\begin{aligned} H_{1\langle r_a r_b \rangle} &= J_z L_{r_a}^z L_{r_b}^z + \zeta \Delta_z [(L_{r_a}^z)^2] \\ &\quad + \zeta \Delta_\perp [(\vec{L}_{r_a}^\perp)^2] - C_{\text{mixed}}, \\ H_{2\langle r_a r_b \rangle}^\pm &= \frac{J_\perp}{2} (L_{r_a}^\pm \cdot L_{r_b}^\mp), \end{aligned} \quad (5)$$

where $\vec{L}_{r_a}^\perp$ denotes the vector made of transverse (x/y) components of $\vec{L}_{r_a} \equiv \vec{S}_{I r_a} + \vec{S}_{II r_b}$ and $\vec{L}_{r_b}^\perp$ denotes the vector made of transverse (x/y) components of $\vec{L}_{r_b} \equiv \vec{S}_{r_b}$, $L_r^\pm = L_r^x \pm i L_r^y$, ζ is the inverse coordination number of the bipartite lattice, C_{mixed} is a constant introduced to ensure that all matrix elements of the *diagonal* operator $H_{1\langle r_a r_b \rangle}$ are negative in our chosen basis, $\Delta_\mu = \mathcal{D}_\mu/2$, and $J_\mu = \mathcal{J}_\mu$ (for $\mu = z, \perp$). Using this decomposition, we have $H_{\text{mixed}} = \sum_{\langle r_a r_b \rangle} H_{1\langle r_a r_b \rangle} + H_{2\langle r_a r_b \rangle}^+ + H_{2\langle r_a r_b \rangle}^-$.

Details for Quantum Monte Carlo simulations of H_{mixed}

The QMC simulations for H_{mixed} use this decomposition to work within the Stochastic Series Expansion using diagonal updates and directed loop updates that change the m quantum number locally during the construction of the loop.

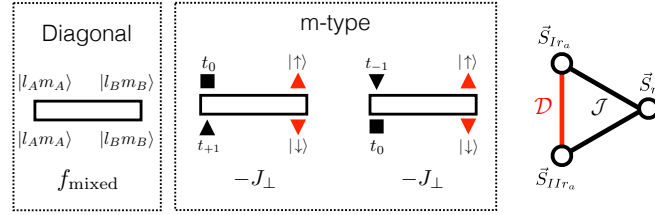


FIG. 5: Vertices that appear in the SSE operator string for H_{mixed} , with corresponding weights in the canonical cluster basis. Other valid vertices are obtained by symmetry operations that exchange upper and lower legs (keeping the weight fixed). The constant C_{mixed} in the function $f_{\text{mixed}}(l_A, l_B, m_A, m_B) = C_{\text{mixed}} - J_z m_A m_B - \zeta(\Delta_z - \Delta_\perp) m_A^2 - \zeta \Delta_\perp l_A(l_A + 1)$ is chosen to ensure that $f_{\text{mixed}} \geq 0$. Right panel: Pictorial representation of the lattice structure and exchange interactions of H_{mixed} .

Explicit demonstration of positive-weight property

For H_{bilayer} , the positive-weight property of our method can be made explicit by switching from the canonical cluster basis to a rotated basis obtained by attaching phase-factors $e^{i\theta_{|lm\rangle} + i\eta_{|lm\rangle}}$ to the states $|l, m\rangle$ of the canonical basis. Here, the $\theta_{|lm\rangle}$ are completely \vec{r} -independent, while the $\eta_{|lm\rangle}$ are 0 on the B sublattice and constant on the A sublattice. These phases are chosen in each of these three generic cases to ensure that every nonzero contribution to the weight in the rotated basis is explicitly positive. For instance, as already mentioned in the main text, when $K_\perp = 0$, we set $\eta_{|t_\pm\rangle} = \theta_{|l, m\rangle} = 0$ (for all l, m), while independently choosing $\eta_{|s\rangle}$ to be 0 or π and $\eta_{|t_0\rangle}$ to be 0 or π depending on the signs of K_z and J_\perp . When $K_z = 0$, we set $\eta_{|t_\pm\rangle} = \theta_{|s\rangle} = 0$, and, depending on the signs of K_\perp and J_\perp , choose $\theta_{|t_0\rangle} = \theta_{|t_\pm\rangle}$ to be either 0 or $\pi/2$, while independently choosing $\eta_{|s\rangle}$ to be 0 or π and $\eta_{|t_0\rangle}$ to be 0 or π . Finally, when $J_\perp = 0$, we set $\eta_{|t_\pm\rangle} = \theta_{|t_0\rangle} = \theta_{|s\rangle} = 0$, and, depending on the signs of K_\perp and K_z , choose $\theta_{|t_+ \rangle} = \theta_{|t_- \rangle}$ to be either 0 or $\pi/2$, while independently choosing $\eta_{|s\rangle}$ to be 0 or π and $\eta_{|t_0\rangle}$ to be 0 or π .

For H_{mixed} , we see from Fig. 5 that the only off-diagonal vertices are m -type vertices (in the terminology used in the main text). Now, as already noted in the main text, the fact that a bipartite lattice only has loops of even length

implies that the number of occurrences of processes that hop the m quantum number must be even in order to satisfy the requirement of periodicity of the operator string. For H_{mixed} , this implies that \mathcal{N}_m be even. This establishes the positive-weight property of our method for H_{mixed} , since any minus signs arising from off-diagonal operators come in pairs. This can be made explicit exactly as in the discussion above for H_{bilayer} , simply by choosing a rotated basis obtained by attaching a phase factor $\eta_{|t_0\rangle}$ that is chosen to be equal to 0 or π depending on the sign of J_{\perp} (all other η and θ are set to zero).

Benchmark results on $d = 1$ systems

Here we present results for two one-dimensional systems that serve as our benchmarks. These are the so-called fully-frustrated ladder and the diamond chain [41, 47]. The former represents the one-dimensional special case of H_{bilayer} with $K_z = K_{\perp} = 0$, while the latter is the one-dimensional realization of H_{mixed} . These results on the benchmarks, together with benchmarking done in the main text for H_{bilayer} in one dimension with $K_z \neq 0$, illustrate that our new QMC method clearly allows us to reliably compute the thermodynamics of large systems over a wide temperature range.

Fully frustrated ladder

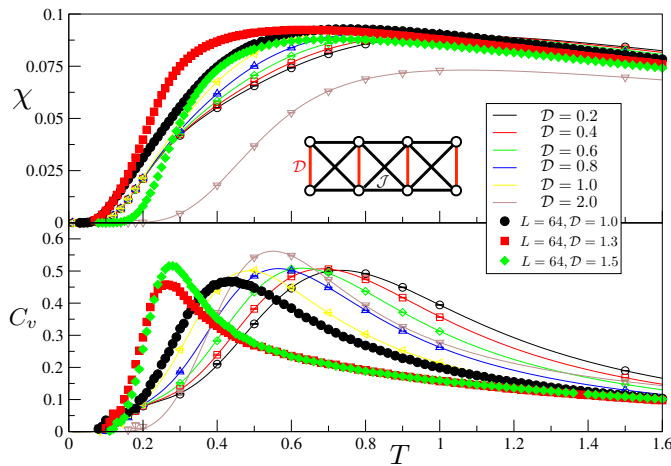


FIG. 6: Susceptibility and specific heat versus temperature for the fully-frustrated ladder, *i.e.* the $d = 1$ bilayer Hamiltonian H_{bilayer} with $J_{\perp} = K_{\perp} = 1$, $J_z = K_z = 1$, and various values of $\mathcal{D}_z = \mathcal{D}_{\perp} \equiv \mathcal{D}$. Solid lines are exact diagonalization results for a small system with $L = 6$, and the corresponding QMC results are depicted by open symbols. Filled symbols are QMC data for a larger ladder of linear size (number of unit-cells) $L = 64$.

As mentioned above, this corresponds to a one-dimensional special case of H_{bilayer} where $K_z = J_z$ and $K_{\perp} = J_{\perp}$ corresponding to the conditions i) and ii) of the main text being both satisfied. In the example of Fig. 6, we set $J = J_z = J_{\perp} = K_z = K_{\perp} = 1$ and vary $\mathcal{D} = \mathcal{D}_z = \mathcal{D}_{\perp}$ (this model has $\text{SU}(2)$ symmetry). The lattice and notations are depicted in the top panel of Fig. 6 for completeness. This figure displays QMC results (symbols) obtained with the algorithm described in the main text for the specific heat C_v and magnetic susceptibility χ for ladders of linear size $L = 6$ and $L = 64$ (containing $2L$ spins $1/2$) with periodic boundary conditions. The $L = 6$ data are displayed to show the perfect agreement with exact diagonalization data for $L = 6$.

Diamond chain

As mentioned above, the diamond chain is a one-dimensional realization of H_{mixed} . Here, we consider the $\text{SU}(2)$ symmetric case, setting $J = J_z = J_{\perp} = 1$ and varying $\mathcal{D} = \mathcal{D}_z = \mathcal{D}_{\perp}$. The lattice is represented in the inset of Fig. 7 for completeness, and contains three spin-half moments per unit cell. Fig. 7 represents the temperature dependence of the magnetic susceptibility for various values of \mathcal{D} for chains with $L = 4$ and $L = 32$ units cells ($N = 12$ and $N = 96$

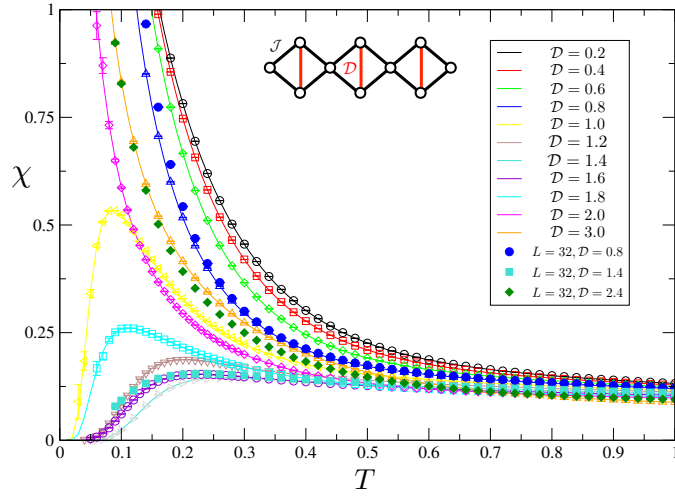


FIG. 7: Susceptibility versus temperature for the special case of H_{mixed} in $d = 1$ (“diamond chain”), with $J_{\perp} = J_z = 1$ for various values of $\mathcal{D}_z = \mathcal{D}_{\perp} \equiv \mathcal{D}$. Solid lines are exact diagonalization results for a small system with $L = 4$ diamond unit cells (*i.e.* $N = 12$ spins), with corresponding QMC data depicted by open symbols. Filled symbols are QMC data for a larger diamond chain with $L = 32$ unit cells.

spins $1/2$ in total), as obtained with the QMC method presented in the main text. The $L = 4$ data match perfectly exact diagonalization results (solid lines).